# Influence of the mapping unit for regional Landslide Early Warning Systems. Comparison between pixels and polygons in Catalonia (NE Spain).

Rosa M Palau [a, b]*, Marcel Hürlimann[b], Marc Berenguer[a], Daniel Sempere-Torres[a]

[a] Center of Applied Research in Hydrometeorology, Universitat Politècnica de Catalunya, Jordi Girona 1-3 (C4), Barcelona 08034, Spain

[b] Division of Geotechnical Engineering and Geosciences, Department of Civil and Enviromental Engineering, Universitat Politècnica de Catalunya, Jordi Girona 1-3 (D2), Barcelona 08034, Spain

Submit to…..Landslides?

Jan 2019

*Corresponding author:

Rosa M Palau

E-mail address: palau@crahi.upc.edu

Phone number:

ORCID: 0000-0002-5350-0522

**Abstract**

This work presents a prototype Landslide Early Warning System (LEWS) adapted to real-time performance over the region of Catalonia (NE Spain). The system uses high-resolution rainfall information obtained from weather radar observations and susceptibility maps to issue a qualitative warning level at a regional scale. To study the influence of the mapping unit on the LEWS outputs, susceptibility maps obtained for Catalonia based on (i) pixels of different sizes and (ii) hydrological subbasins have been compared. The susceptibility has been derived using a simple fuzzy logic approach combining slope angle and land cover data. The susceptibility maps for the different mapping units have then been employed to run the LEWS for a period of 7 months (warm season of 2010). For each configuration, the performance, interpretability of the warnings and, computational requirements have been compared to assess the suitability of each mapping unit for their use in the LEWS in real time. The configuration using pixels of 30 m resolution as mapping units seems to be the best as a compromise between resolution, performance and computational cost. However, from an end-user's real-time perspective the interpretation of the warnings can be difficult. Therefore, summarizing and visualizing the warnings, which are computed over the high-resolution grid, by subbasins is proposed as the best option.

KEYWORDS: Landslides, Early Warning Systems, mapping units, susceptibility analysis.

## 1. Introduction

Rainfall-triggered shallow slides and debris flows represent an important hazard that causes major economic losses and fatalities worldwide (e.g. Jakob and Hungr 2005; Froude and Petley 2018). Although these phenomena are not as widely reported in Catalonia (NE Spain) as they are in other regions, their hazard is still significant (Gallart and Clotet 1988; Portilla et al. 2010a; Hürlimann et al. 2014; Palau et al. 2017). Rainfalls that trigger shallow slides and debris flows are frequently rather short and intense (Guzzetti et al. 2008; Alfieri et al. 2012; Abancó et al. 2016) and its frequency is expected to increase due to climate change (Gariano and Guzzetti 2016). Building reliable Early Warning Systems is of key importance to reduce the risk by increasing awareness and preparedness of communities which may be exposed (Alfieri et al. 2012; UNISDR 2015; Alcántara-Ayala et al. 2017).

In the recent years, regional Landslide Early Warning Systems (LEWS) have been developed covering multiple areas worldwide; e.g. Japan (Osanai et al. 2010), Hong Kong (Lloyd et al. 2001), the Chinese Zhejiang province (Yin et al. 2008), Southern California (Baum and Godt 2010), Rio de Janeiro (Calvello et al. 2014), the Italian regions of Emiglia-Romana and Campania (Piciullo et al. 2017; Segoni et al. 2018), Norway (Krøgli et al. 2018) and the Catalan Pyrenees (Berenguer et al. 2015). These LEWS frequently use susceptibility maps to depict the landslide prone areas and assess whether a rainfall event might trigger a landslide by means of rainfall thresholds (Aleotti 2004; Baum and Godt 2010; Papa et al. 2013; Berti et al. 2015; Piciullo et al. 2017; Pan et al. 2018). The quality of both the susceptibility assessment and the rainfall data (as well as the rainfall Intensity-Duration thresholds) influence significantly the accuracy of the issued warnings.

Generally, the rainfall inputs are obtained from rain-gage measurements (Piciullo et al. 2017; Krøgli et al. 2018; Segoni et al. 2018). But in many cases the density of rain-gage networks is low, especially in remote mountainous areas, and landslide triggering rainfalls tend to be underestimated (Marra et al. 2014). For this reason, some large scale (regional or global) LEWS use radar rainfall

observations (NOAA-USGS Debris Flow Task Force 2005; Chen et al. 2007; Osanai et al. 2010; Berenguer et al. 2015) or satellite rainfall products (Rossi et al. 2017; Kirschbaum and Stanley 2018).

Susceptibility maps describe the spatial distribution of the likelihood of having a landslide (Fell et al. 2008). When implemented into a LEWS they are used to identify the locations where future events are more likely. Susceptibility maps relate landslide occurrence with a number of variables that control its initiation. However, obtaining high-resolution information of certain geotechnical variables directly related to landslide occurrence at regional scale is very difficult. As a consequence, susceptibility is usually characterized using morphological parameters obtained from digital elevation models (DEMs), and sometimes also include geological and land cover information (Chevalier et al. 2013; Leopold et al. 2013; Liu et al. 2013; Bregoli et al. 2015; Kirschbaum et al. 2016; Wilde et al. 2018).

Susceptibility zoning is based on the discretization of the study region into homogeneous mapping units (Hansen 1984). Diverse mapping units have been used to report warnings, for example polygons (municipalities, catchments…), lines (roads) or pixels (Lloyd et al. 2001; Liao et al. 2010; Huat et al. 2012; Berenguer et al. 2015; Krøgli et al. 2018; Segoni et al. 2018). Choosing an appropriate mapping unit for LEWS is not straightforward and requires considering several factors such as the resolution, the accuracy of the warnings, end-users' interpretability of the results, and computational cost. In the past, some authors have studied the effect of using polygon or grid-cell mapping units in the performance of susceptibility assessments (Carrara et al. 2007; Calvello et al. 2013; Hürlimann et al. 2016). However, there is still no study on its influence on the performance of a LEWS.

The aim of this paper is twofold: (i) assessing the influence of the mapping unit on the outputs of a regional LEWS, and (ii) selecting the most suitable mapping unit for a regional LEWS for Catalonia adapted to real-time performance. This has required the retrieval of the susceptibility map for Catalonia, which is a secondary goal of the presented work.

## 2. Settings

### *2.1. Geographic, Geologic and Climatic Settings*

The region of Catalonia is located at the NE of Spain and covers an area of around 32000 km$^2$. Its altitude ranges from sea level to 3143 m in the Pyrenees. From a geological point of view, Catalonia is located at the Iberian Plate. Its orography is the result of (i) the collisions of the Iberian Plate, the European Plate and the African Plate during the Paleogene, forming the Pyrenees, the Catalan Coastal Range and the Iberian Range, (ii) the deposition of its sediments in the Ebro Basin depressions, and (iii) the reactivation of pre-existing faults in an extensive context during the Miocene, forming a series of horsts and grabens more or less parallel to the actual coast-line (Berastegui et al. 2010).

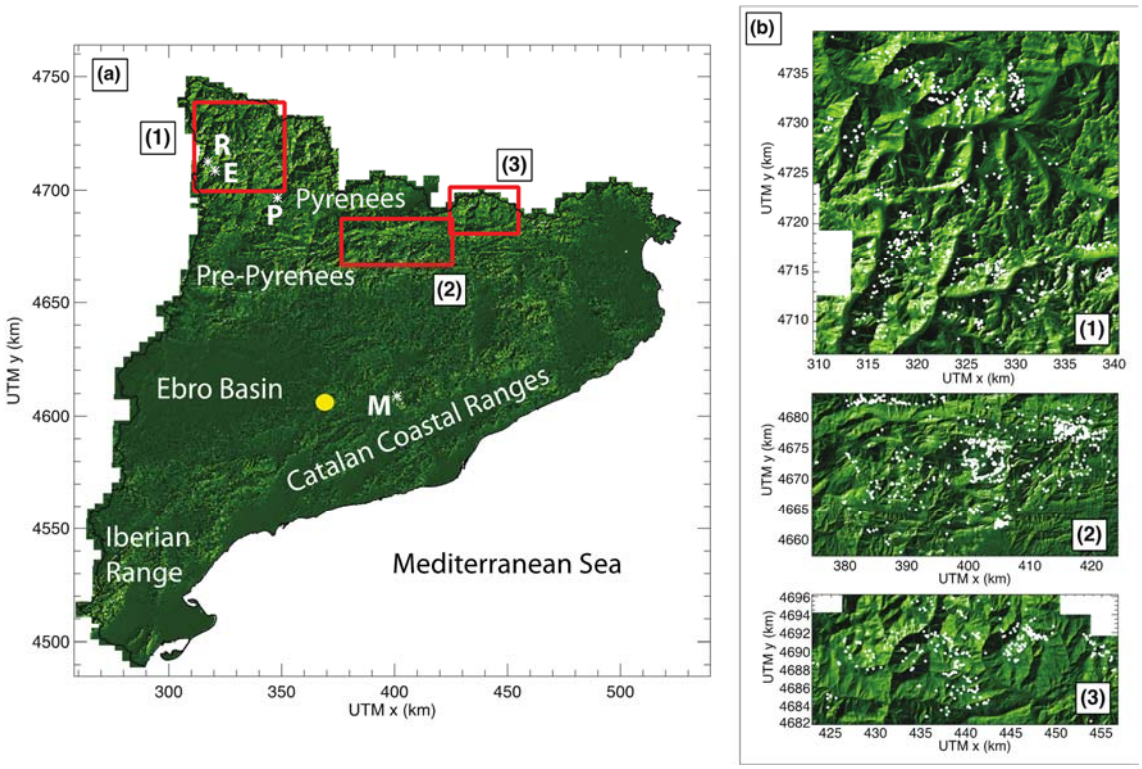


**Fig. 1.** (a) Overview map of Catalonia. The red rectangles show the areas where landslide inventories exist in (1) NW-Catalonia, (2) NC-Catalonia and (3) NE-Catalonia. The yellow circle represents the location of the CDV C-band weather radar. R, E, P and M show, respectively, the locations of Rebaixader, Erill, Portainé and Santa Maria, where landslide events were reported during 2010 (see section 5). (b) Inventory of landslide locationsin the three areas shown with the red rectangles in panel a).

110 Catalonia's climate is varied but can be classified as Mediterranean (Mira et al. 2017). Near the
111 coast the climate is mild and temperate. Inland, the climate is continental, with cold winters and
112 hot summers. The Pyrenees present a high-altitude climate, with abundant snow and temperatures
113 below 0ºC during winter. The rainiest seasons are generally spring and autumn with the exception
114 of the Pyrenees where the rainiest season is summer. The majority of the landslides are triggered
115 by either (i) convective rainfall events with high intensities, which are typical from mid-summer to
116 early autumn, and (ii) long-lasting rainfalls with moderate intensities, common during spring and
117 autumn (Corominas et al. 2002; Abancó et al. 2016).

118 *2.2. Datasets used*

119 The majority of LEWS methods use susceptibility and rainfall information. Here, we describe
120 the data that has been used to implement our prototype LEWS. A full description of the method
121 is presented in in section 3.

122 The rainfall datasets used in this study are radar-based Quantitative Precipitation Estimates
123 (QPE). Specifically, 30-min rainfall accumulations with a spatial resolution of 1 km. These maps
124 have been produced with the Integrated Tool for Hydrometeorological Forecasting (EHIMI,
125 Corral et al. 2009) from the volume scans of the Creu del Vent single-polarization C-band Doppler
126 radar of the Meteorological Service of Catalonia (SMC). The location of the radar is shown in **Fig.**
127 **1**. The EHIMI tool includes a chain of correction and quality control algorithms to generate the
128 QPE products from raw radar observations.

129 To derive the susceptibility maps, the 5 m resolution DEM of Catalonia (ICGC 2013) has
130 been used. Additionally, information on land use and land cover (LULC) has been obtained from
131 the Map of Soil Coverage of Catalonia (MCSC-4, CREAF 2009).

132 Information of historic and recent shallow slides and debris flows contained in the inventories
133 of three zones located in the Pyrenees and the Pre-Pyrenees (**Fig. 1**b, **Table 1**)has been used for the
134 susceptibility assessment. The NW-Catalonia inventory is the most recent and accurate and consists

of 908 events. These events were principally identified by means of interpretation of aerial photos, and both 2D and 3D digital orthophotos (Chevalier 2013; Shu et al. 2019). The NC-Catalonia inventory is composed of 1249 landslide events. The majority of these events were triggered by the extraordinary rainfall episode of 7-8 November 1982 and were geolocalized on topographic maps during field surveys and photointerpretation (Gallart and Clotet 1988). The spatial accuracy of this inventory is the lowest. Finally, the NE-Catalonia inventory contains 317 landslides. Many of them were triggered by the catastrophic October 1940 rainfall event and the geolocalization of these landslides was done by analysis of the 1956-1957 aerial photographs taken by the Spanish Army Geographical Service (Portilla Gamboa 2014). Further details about the three inventories and its analysis can be found in Hürlimann et al. (2016).

**Table 1.** Summary of the characteristics of the three inventory areas

| Study Area | Main lithology | Area [km$^2$] | # of landslides | Average density [# of landslides per km$^2$] |
|---|---|---|---|---|
| NW-Catalonia | Igneous & Metamorphic | 1018 | 908 | 0.89 |
| NC-Catalonia | Sedimentary | 1317 | 1249 | 0.95 |
| NE-Catalonia | Igneous & Metamorphic | 486 | 317 | 0.65 |

## 3. General methodology

The prototype LEWS applied in this study has been designed with the aim of working in realtime and has the purpose of issuing warnings to the authorities in charge of managing the risk. It is based on the scheme developed by Berenguer et al. (2015), which was applied in two study areas in the Catalan Pyrenees. Its inputs are (i) susceptibility information, and (ii) gridded rainfall observations. The output of the LEWS is a map showing a qualitative warning level ("very low",

153 "low", "moderate" and "high") for each mapping unit every time new rainfall observations are
154 available (in this case every 30 min, see section 2.2). **Fig. 2** shows a general scheme of the system.
155 Its components are shown in the sections below.

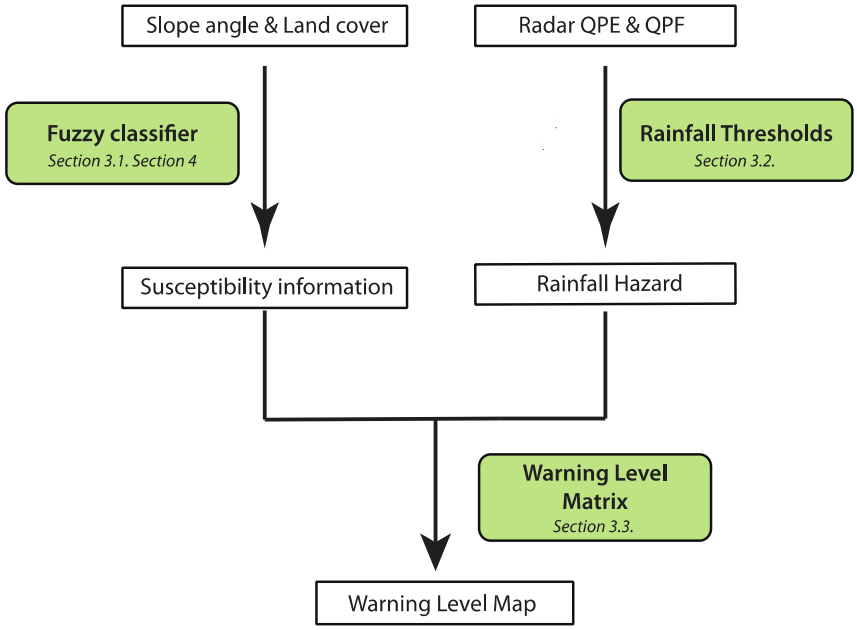


156

157 **Fig. 2.** General flow chart of the prototype LEWS algorithm.

158 *3.1. Susceptibility analysis*

159 A static susceptibility map is used by the LEWS to distinguish landslide-prone areas. The
160 susceptibility map for Catalonia has been derived combining the slope angle and land cover. The
161 method used for susceptibility mapping (similar to that of Berenguer et al. (2015)) is described in
162 detail in section 4. It employs fuzzy logic (Mendel 1995) to classify the susceptibility in four
163 categories: "very low", "low", "moderate" and "high".

164 *3.2. Characterization of the rainfall hazard level*

165 Rainfall intensity-Duration (I-D) relationships are widely used in LEWS to assess the hazard
166 posed by a rainfall situation. In Catalonia no comprehensive I-D thresholds are available, only
167 preliminary rainfall thresholds based on daily rainfall records or thresholds at catchment scale exist
168 (e.g., Corominas 2000; Abancó et al. 2016). Thus, to asses the magnitude of rainfall situations in
169 the analysis domain, we have used the intensity-duration-frequency (IDF) curves of the Fabra

meteorological observatory in Barcelona (Casas et al. 2004) as reference. The IDF curves are the base to define four rainfall hazard levels: "very low", "low", "moderate" and "high" (**Fig. 3**). The definition of the thresholds has been done empirically with the following criteria: for the high rainfall hazard, the I-D curve for a return period of 5 years has been used. In addition, the two other thresholds (lower limit of hazard level "moderate" and "low") were defined as parallel I-D curves that are below the two years return period. Although these thresholds do not directly relate rainfall with landslide occurrence, their slopes are very similar to the ones of local rainfall thresholds obtained for specific sites in Catalonia (e.g. Abancó et al. 2016; Hürlimann et al. 2017).

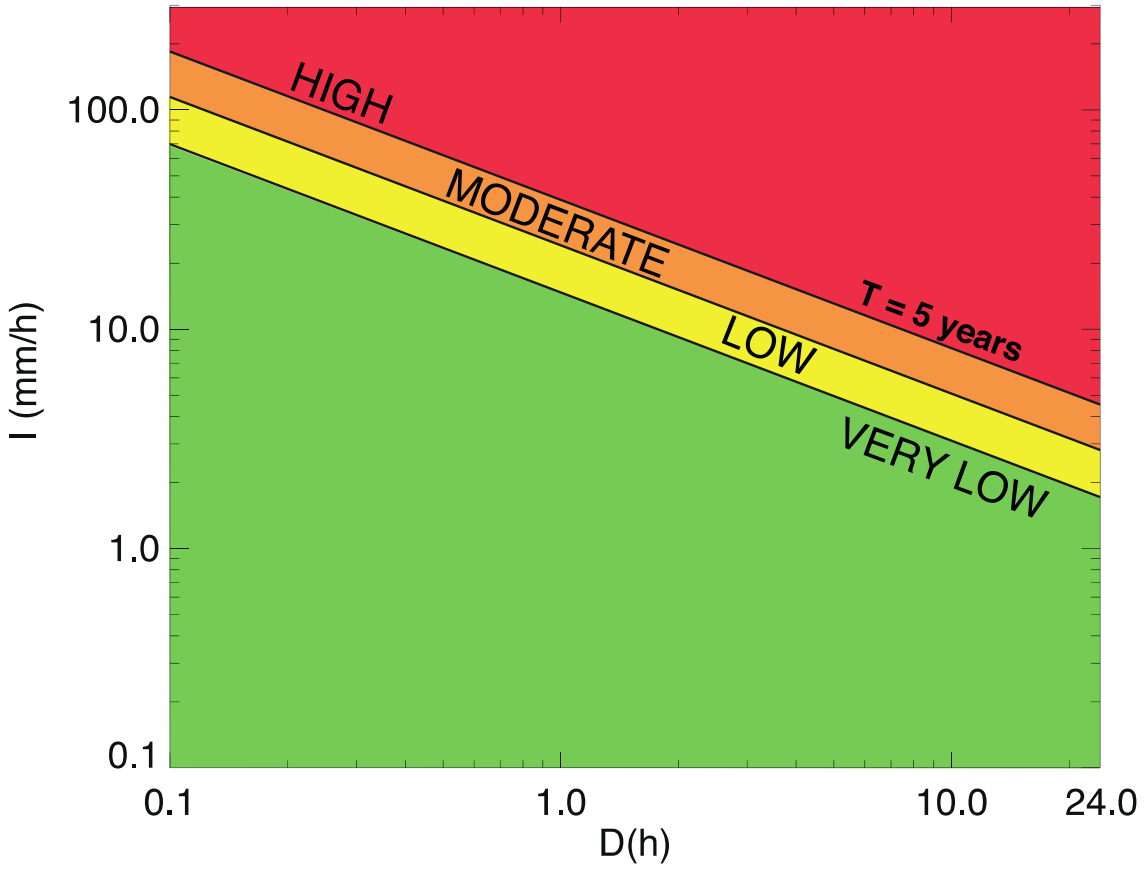


**Fig. 3.** Rainfall intensity-duration thresholds. The background green, yellow, orange and red colors represent the four rainfall hazard level classes: "very low", "low", "moderate" and "high".".

### *3.3. Definition of the warning level*

Combining the susceptibility of the mapping unit and the magnitude of the rainfall event, the LEWS issues a warning. While susceptibility is considered to be static (it remains constant in time),

184 rainfall inputs are updated every 30 minutes. The combination of the susceptibility and rainfall
185 hazard is done according to the warning level matrix of **Fig. 4.** The result for each timestep is a
186 qualitative warning level for each mapping unit of one of the following four classes: "very low",
187 "low", "moderate" and "high".

188 Each warning level class aims at assessing the possibility of having a shallow slide or debris
189 flow; i.e. increasing the warning level implies increasing the probability of the expected event.

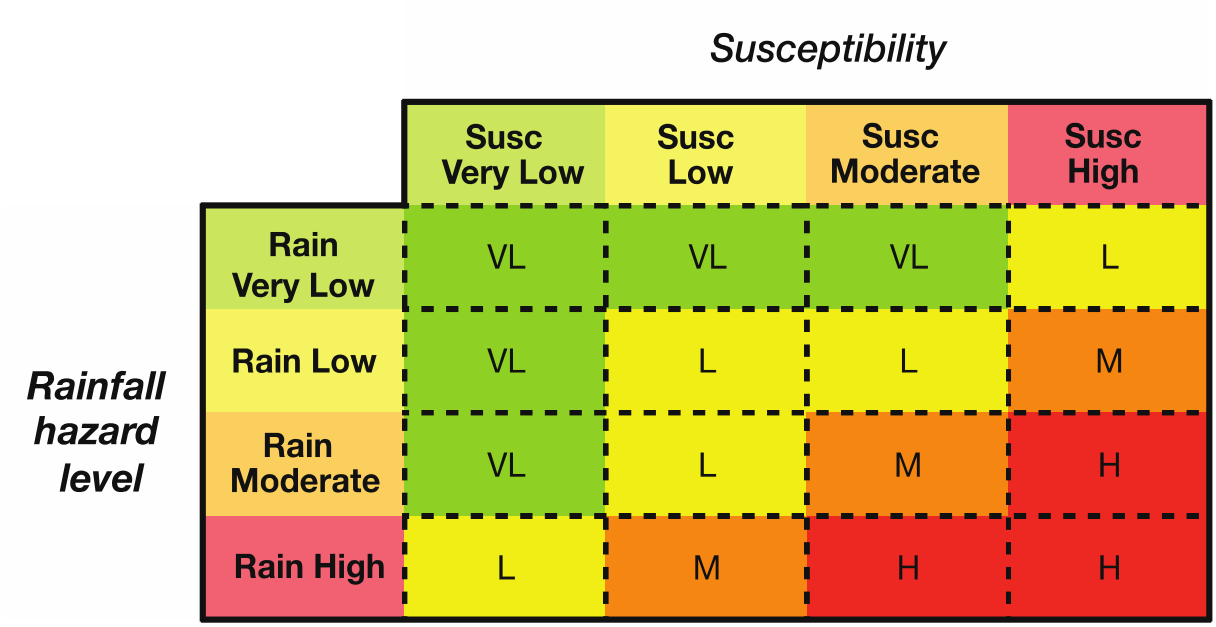

190

191 **Fig. 4.** Warning level matrix. Rows represent the rainfall hazard level; columns represent the susceptibility degree. "VL", "L", "M" and "H"
192 stand for "very low", "low," "moderate" and "high" warning level respectively.

193 ## 4. Susceptibility map of Catalonia

194 One of the requirements to extend the LEWS to Catalonia is mapping the susceptibility over
195 the entire region. Up to the date there is no susceptibility assessment spanning the whole region.
196 This section first presents the methodology used to derive the susceptibility map with different
197 mapping units, and next, the different susceptibility maps are evaluated by (i) visual inspection, and
198 (ii) from a quantitative point of view in a validation framework.

199 ### *4.1. Susceptibility mapping methodology*

200 Chevalier et al. (2013) analyzed the skill of different morphological parameters obtained from

201 the DEM to assess shallow slides and debris flows susceptibility. Their results showed that the
202 most significant governing factor was the terrain slope angle. Though, they did not include
203 information associated with the soil layer in their analysis. Some authors (Nadim et al. 2006; Ciurleo
204 et al. 2016; Wilde et al. 2018) have used information contained in geological maps to assume
205 geotechnical properties of the soil. However, in Catalonia, the geological map mostly lacks
206 information on surficial formations. Thus, a reasonable alternative consists in using land use and
207 land cover (LULC) information, as proposed by several authors (e.g. Hürlimann et al. 2016; Pisano
208 et al. 2017; Gariano et al. 2018). LULC provide indirect information of sediment availability. In
209 addition, the vegetation plays an important role in slope stability [e.g. evapotranspiration, suction,
210 apparent cohesion given by the plant roots (Schmidt et al. 2002; Schwarz et al. 2010)]. The removal
211 of vegetation generally increases susceptibility (Persichillo et al. 2017; Pisano et al. 2017). For these
212 reasons, the susceptibility map of Catalonia presented herein has been derived using slope angle
213 and LULC, which are datasets currently available not only in Catalonia, but also in most countries.

214 Susceptibility maps of two main types have been derived: (i) raster grids of different resolutions
215 (5 m, 30 m, 200 m and 1 km), and (ii) a subdivision of the analysis domain in hydrological subbasins
216 (including 1$^{st}$, 2$^{nd}$ and 3$^{rd}$ order , following the method of Strahler, 1957). The mean area and its
217 standard deviation of these subbasins are 2.1 km$^2$ and 1.6 km$^2$ respectively. For the map based on
218 raster grids, the 5 m DEM has been upscaled to obtain the DEMs of lower resolutions and the
219 slope angle of each resulting cell has been computed using GIS tools.

220 The 241 original land cover classes of the LULC map have been reclassified into 11 classes
221 that were significant in terms of slope stability following the Corine Land Cover Classification
222 (EEA 1990). As the original land cover map was rasterized at a resolution of 5 m, we had to adopt
223 a criterion to upscale the information to 30 m, 100 m, 200 m and 1 km resolutions and subbasins.
224 Finally, we have chosen to assign the most susceptible land cover class to the larger mapping unit,
225 on the condition that this class is representative enough (it occupies at least 15% of the (larger)
226 terrain unit). This methodology is quite feasible, but decreases land cover variability with decreasing

227 resolution and biases it towards more susceptible classes as it can be seen in **Fig. 5**.

228 Slope angle and land cover have been combined to retrieve the susceptibility maps using a
229 fuzzy logic classifier (Mendel 1995). Compared to statistical methods, fuzzy logic has the following
230 advantages: (i) it is able to model the non-linear behavior of the susceptibility input variables, (ii) it
231 uses expert criteria to assess the uncertainty of input parameters and landslide inventories, (iii) it is
232 simple and can be easily adapted to different regions.

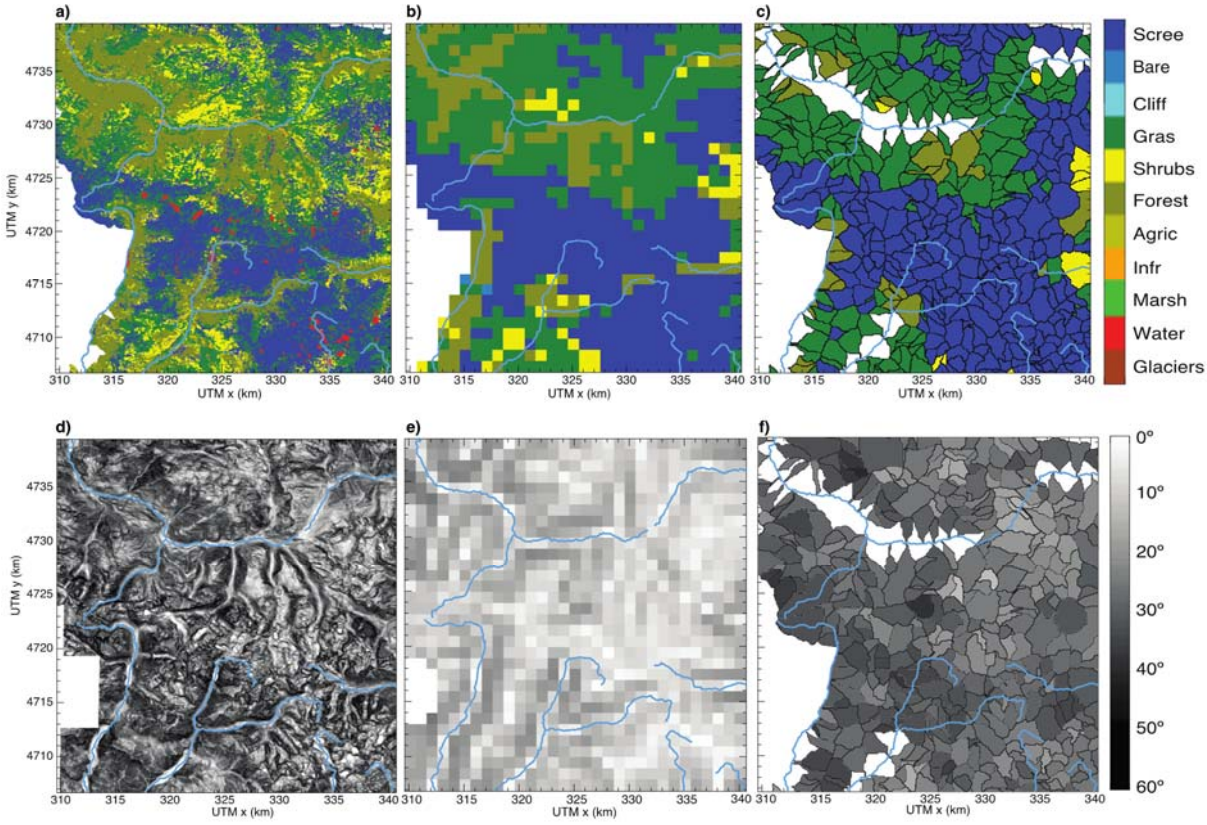


233

234 **Fig. 5.** Maps of the NW-Catalonia study area. The upper and the bottom rows show respectively the land cover
235 maps and the slope angle maps with pixel resolution of (a), (d) 30 m, (b), (e) 1 km and, (c), (f) hydrological subbasins
236 respectively.

237 The used fuzzy logic classifier requires a weight for each input variable (slope and land cover)
238 and membership functions for each input variable and each susceptibility class ("very low", "low",
239 "moderate" and "high"). Membership functions measure how realistic it is that a mapping unit
240 where one variable takes a value $x$ belongs to a certain susceptibility class. Here, similarly as
241 Berenguer et al. (2015), the membership functions and weights for the slope angle and the land

242 cover have been designed by an expert using subjective criteria by taking the information of
243 landslide frequency distributions of a random sub-set containing half of the points of the landslide
244 inventory as a reference (not shown). Slope angle membership functions have been adapted for all
245 the different mapping units (**Fig. 6**a-**Fig. 6**c). In contrast, land cover landslide frequency
246 distributions are very similar for all the mapping units; and thus, the same membership functions
247 set has been adopted for all mapping units (**Fig. 6**d).

248 From these membership functions, the membership degree to a susceptibility class ($M_S$)
249 assesses the feasibility that a mapping unit belongs to it. Its value ranges from zero to one and has
250 been computed as follows:

251 $$M_S = w_{sl}\,\mu_{sl,S} + w_{lc}\,\mu_{lc,S} \qquad (1)$$

252 where $w_{sl}$ and $w_{lc}$ are the weights of slope and land cover respectively, and $\mu_{sl,S}$ is the
253 membership degree for the slope and for a susceptibility class S, $\mu_{lc,S}$ is the land cover membership
254 degree for a susceptibility class S.

255 The susceptibility class having the highest membership degree (i.e. higher possibility of having
256 landslides) has been assigned to each terrain unit. That is:

257 $$S = argmax\,\{M_{VL}, M_L, M_M, M_H\} \qquad (2)$$

258 where S states for the susceptibility class, and $M_{VL}, M_L, M_M, M_H$ for the membership degree
259 of the classes "very low", "low", "moderate" and "high" respectively.

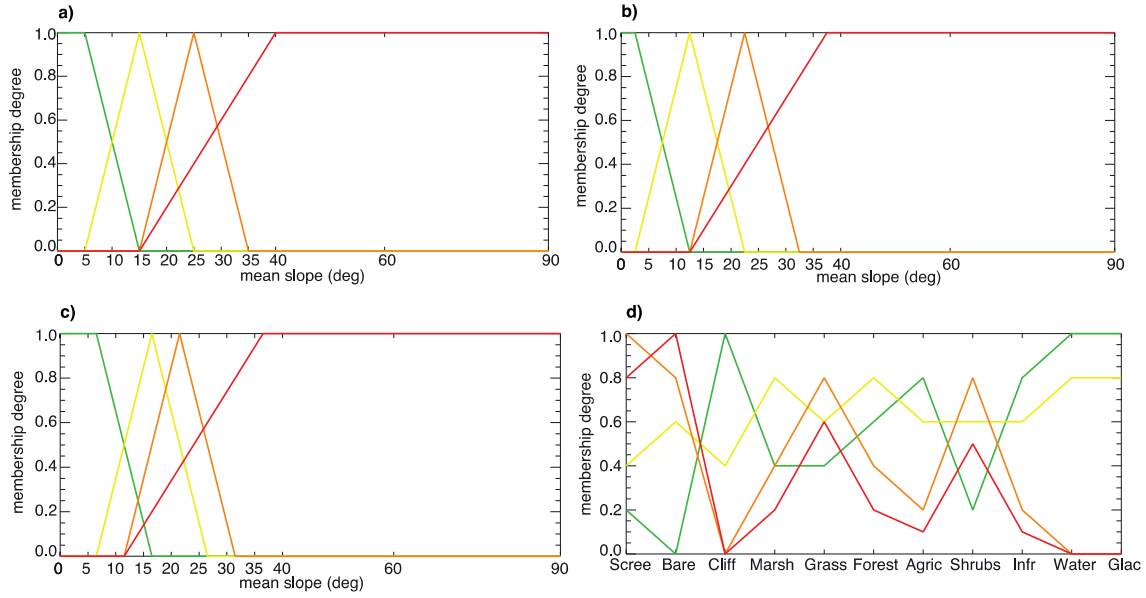


**Fig. 6.** Slope membership functions for pixels with a resolution of (a) 30 m, (b) 200 m, and (c) hydrological catchments. (d) Land cover membership functions. Green, yellow, orange and red lines represent the membership functions of "very low", "low", "moderate" and "high" susceptibility.

### *4.2. Comparing the different susceptibility maps*

The fuzzy logic classifier has been applied to create landslide susceptibility maps covering the region of Catalonia using 5 m, 30 m, 100 m, 200 m, 1 km grid-cells, and subbasins as mapping units. The susceptibility map based on 30 m grid-cells shows variability, with the areas having higher susceptibility located in the mountainous regions of the Pyrenees and the Catalan Coastal Ranges (**Fig. 7**). The flat areas of the low Ebro Basin generally present "very low" susceptibility. The results for the other mapping units (not shown here) are relatively similar.

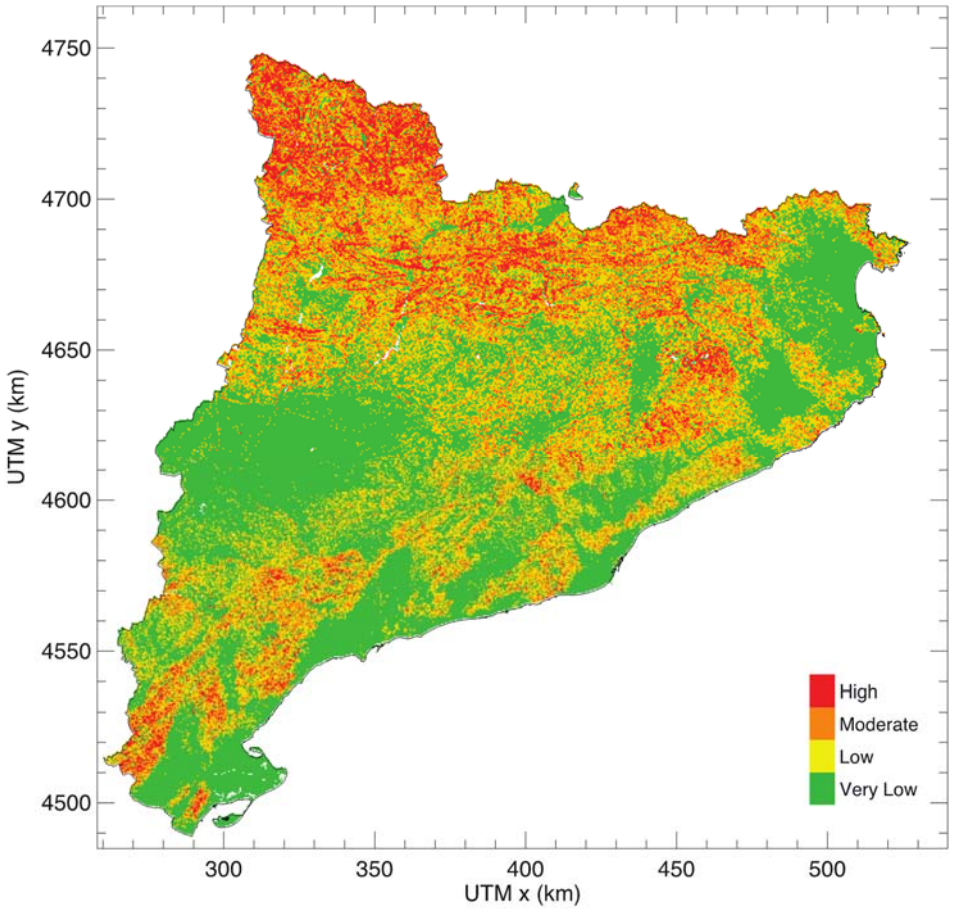


**Fig. 7.** Susceptibility map of the Catalonia using 30 m grid-cells as mapping units.

The resulting susceptibility maps based on the different mapping units for the NW-Catalonia zone are shown in **Fig. 8**. In this area located in the Axial Pyrenees, the 5 m, 30 m, 100 m and 200 m pixels susceptibility maps include large parts of "moderate" and "high" susceptibility.

Unlike pixel-based susceptibility maps, the susceptibility map of hydrological subbasins does not cover the entire domain and classifies almost all the mapping units in the NW-Catalonia zone as "moderate" and "high" susceptibility (**Fig. 8**f). However, the percentage of area occupied by these two classes is similar to the area occupied by the same two classes in the map that uses pixels of 5 m resolution as mapping units (**Table 2**). The main difference relies on the percentage of area classified as "very low" and "low" susceptibility class which is much smaller for the map of subbasins. This can be partly explained because the subbasin map covers mainly the upstream parts of the domain where slope is generally steeper and therefore typically it corresponds to areas that are more susceptible.

285 Regarding the three inventory subdomains (presented in section 2.2 and in **Fig. 1**), the area
286 occupied by moderate and high susceptibility grid cells reduces with decreasing resolution to the
287 point that the map of 1 km pixels classifies more than half as "very low" and "low" susceptibility.

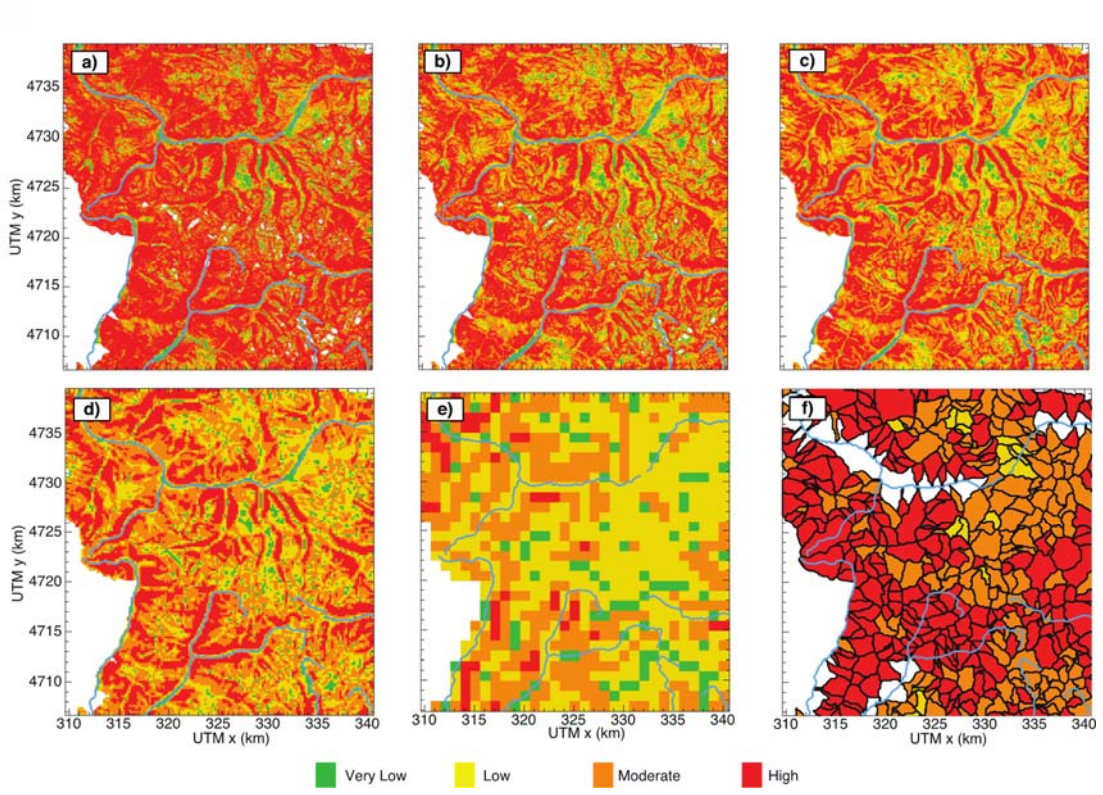


288

289 **Fig. 8.** Susceptibility maps of the NW-Catalonia study area. (a) 5m, (b) 30 m, (c) 100 m, (d) 200 m and (e) 1 km
290 grid-cells, and (f) hydrological subbasins

291 **Table 2** Area (in km$^2$) occupied by each susceptibility class at the NW-Catalonia zone for the susceptibility maps based
292 on the different mapping units. The percentage of the NW-Catalonia domain covered by each class is displayed in
293 parentheses. Note that the total area occupied by hydrological subbasins is smaller than the area occupied by the rest
294 of mapping units.

| | Subbasins | Pixels 5 m | Pixels 30 m | Pixels 100 m | Pixels 200 m | Pixels 1 km |
|---|---|---|---|---|---|---|
| Very Low | 0 (0%) | 58 (6%) | 64 (7%) | 49 (5%) | 50 (6%) | 91 (10%) |
| Low | 30 (3%) | 103 (12%) | 171 (18%) | 187 (20%) | 235 (25%) | 463 (50%) |
| Moderate | 319 (34%) | 187 (20%) | 292 (32%) | 340 (37%) | 399 (25%) | 325 (35%) |
| High | 501 (53%) | 575 (62%) | 402 (43%) | 358 (38%) | 253 (42%) | 49 (5%) |

295

296 *4.3. Validation of the susceptibility maps*

297 The resulting susceptibility maps have been evaluated using the landslide data that were not
298 used for the calibration (i.e. retrieval of the membership functions and weights). The evaluation
299 has been done with Receiver Operating Characteristics (ROC) curves (Fawcett 2006): For each
300 susceptibility class, the false positive rate (fpr) and the true positive rate (tpr) have been computed,
301 and the area under the curve (AUC) is the metric that has been used to assess the model
302 performance. The AUC is a measure of how well a susceptibility classifier can distinguish between
303 mapping units with and without landslide observations. The perfect discriminant is a susceptibility
304 classifier that achieves an AUC equal to one. The larger the AUC, the better is the classification of
305 the susceptibility map.

306 Our results show that generally, the AUC of the grid-cell susceptibility maps slightly decreases
307 with decreasing resolution. Combining the three inventory zones its AUC-values range from 0.59
308 to 0.67 (**Fig. 9** and **Table 3**). The smallest AUC is obtained for the susceptibility map based on 1
309 km grid-cells. In general, the results in the NC-Catalonia zone are the worst, with AUC values
310 ranging from 0.52 to 0.56 (**Fig. 9** and **Table 3**). On the other hand, the region with the highest AUC
311 values is the NW-Catalonia zone where the most complete and recent inventory is available.

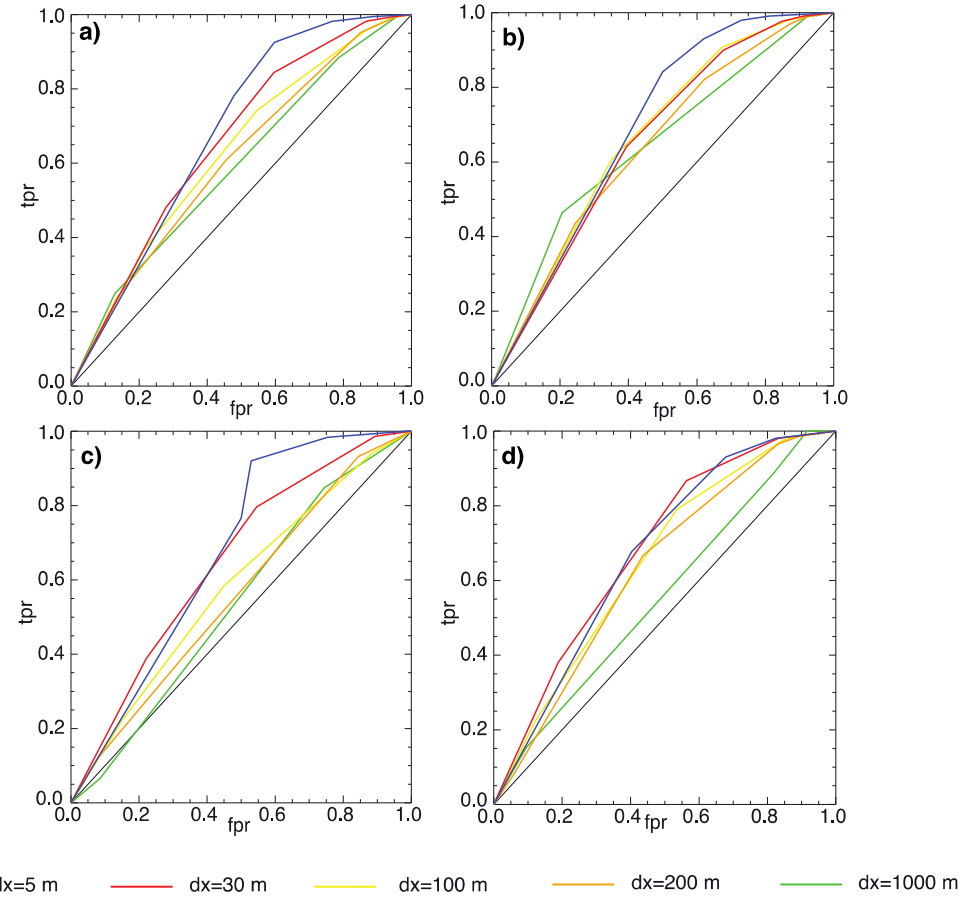


**Fig. 9.** ROC curves of the 5 m, 30 m, 100 m, 200 m, and 1 km grid-cell based susceptibility maps at (a) NW-Catalonia, (b) NC-Catalonia zone. (c) NE-Catalonia zone and (d) all zones. The horizontal axis represents the false positive rate (fpr), the vertical axis represents the true positive rate (tpr).

The comparison of grid-cell based susceptibility maps that cover all the analyzed domain, and subbasin-based susceptibility maps that cover only part of it is challenging. To do so, pixel-based maps have been clipped with the catchments polygons. The resulting grid-cell susceptibility maps covered the same area as the subbasin susceptibility maps and were validated using ROC analysis.

Consistently, the AUC of the clipped grid-cell susceptibility maps decreases with decreasing resolution. The smallest AUCs of the clipped grid-cell and the subbasin-based susceptibility maps are obtained in the NC-Catalonia domain (**Table 3**). As it can be seen in **Fig. 10** and **Table 3** the subbasin-based map performance is slightly better than the performance of 100 m grid-cell susceptibility map and it only achieves a smaller AUC in the NW-Catalonia zone.

325 **Table 3** AUC values obtained from ROC analysis of the susceptibility maps based on the different mapping units.
326 Values in bold are the highest AUC values in each inventory zone.

| Pixel size [m] | AUC | | | |
|---|---|---|---|---|
| | All Zones | NW-Catalonia | NC-Catalonia | NE-Catalonia |
| Over the domain defined by grid-cells | | | | |
| 5 | **0.67** | **0.68** | 0.56 | 0.65 |
| 30 | 0.66 | 0.64 | **0.66** | **0.67** |
| 100 | 0.63 | 0.65 | 0.59 | 0.63 |
| 200 | 0.61 | 0.63 | 0.57 | 0.62 |
| 1000 | 0.59 | 0.65 | 0.52 | 0.55 |
| Over the domain defined by subbasins | | | | |
| 5 | **0.66** | **0.67** | 0.59 | 0.67 |
| 30 | 0.65 | 0.64 | **0.66** | 0.67 |
| 100 | 0.62 | 0.66 | 0.58 | 0.64 |
| 200 | 0.61 | 0.63 | 0.55 | 0.62 |
| Subbasins | 0.63 | 0.63 | 0.58 | **0.69** |

327

328 Therefore, for both, the domain defined by grid-cells and the domain defined by subbasins,
329 the best susceptibility map is the one based on 5 m resolution pixels. The poor results obtained in
330 the NC-Catalonia zone can be, at least partly, explained by the lower quality of the landslides
331 inventory in this domain (especially in the accuracy of the landslides location). Apart from the map
332 based on 1 km grid-cells, the obtained susceptibility maps have an acceptable performance and
333 could therefore be used for LEWS.

334

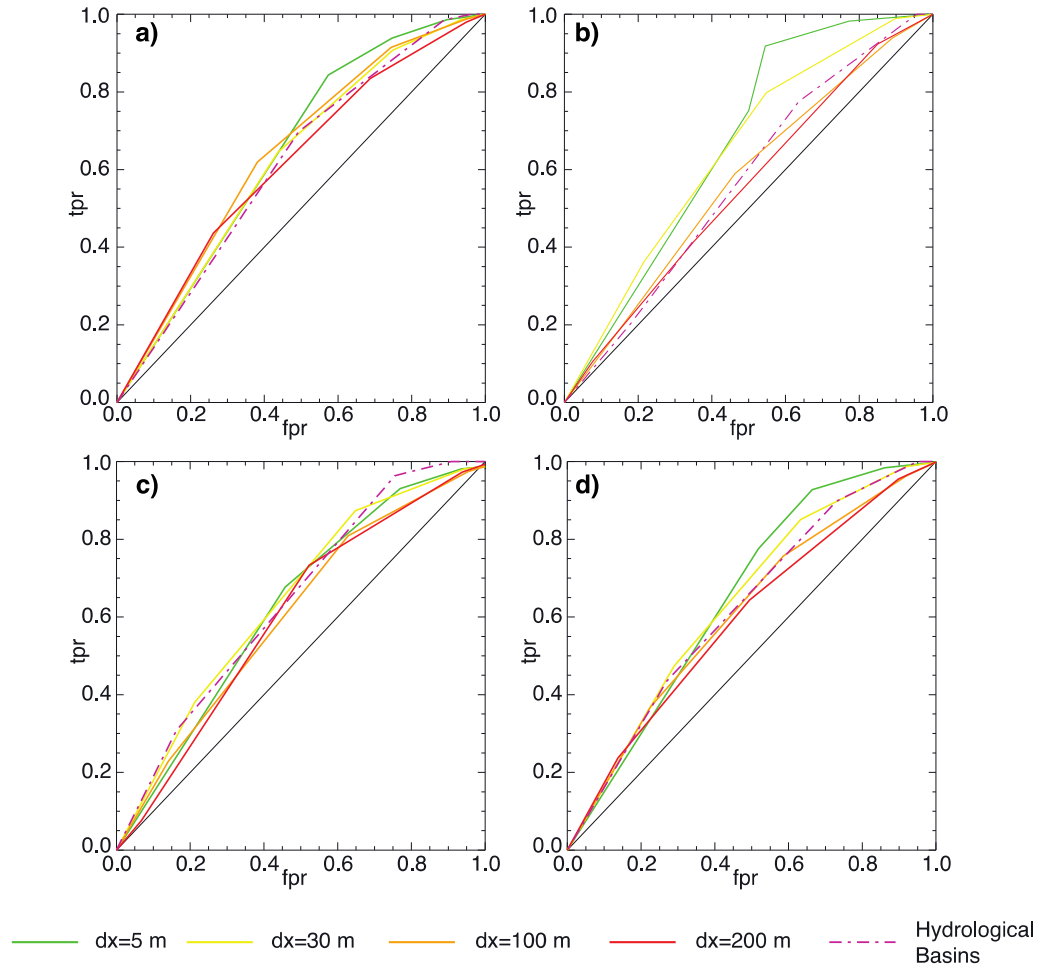


335

336 **Fig. 10.** ROC curves comparing the performance of the susceptibility maps over the area occupied by hydrological
337 catchments. (a) NW-Catalonia, (b) NC-Catalonia, (c) NE-Catalonia, (d) three inventory zones. The horizontal axis
338 represents the false positive rate (fpr), the vertical axis represents the true positive rate (tpr).

339 ## 5. Performance of the LEWS with the different mapping units

340 In this section, the LEWS presented in Section 3 has been run from April to October 2010 to
341 analyze the effect of the mapping units on the landslide warnings over Catalonia. With this aim,
342 the LEWS has been set up using the different mapping units for which the susceptibility maps have
343 been obtained in section 4. Specifically, the analyzed mapping units are (i) 30 m grid-cells, (ii) 200
344 m grid-cells, and (iii) hydrological subbasins. Running the LEWS using 5 m grid cells is still
345 computationally too expensive and this configuration has been discarded in this part of the analysis.
346 The LEWS time resolution is 30 min for all the tested set-ups.

347 The performance of the LEWS with the different configurations has been analyzed in terms
348 of (i) the number of days with warnings for the different mapping units, (ii) its ability to identify
349 the occurrence of specific events that took place during the studied period and for which the exact
350 or approximate triggering time is known. Finally, some discussion about the computational cost to
351 run the LEWS with the different mapping units is provided.

352 *5.1. Number of warnings during the studied period*

353 The total number of days during which "moderate" or "high" warning levels were issued at
354 least once for each mapping unit is summarized in **Fig. 11**. The results show that the areas where
355 these warnings were issued coincide with the zones of "high" susceptibility mostly located in the
356 Pyrenees and Pre-Pyrenees.

357 The 30 m grid-cells configuration issued a "moderate" or "high" warning level during more
358 than six days in over 0.09 % of Catalonia (**Table 4**). This percentage of area is higher for the setup
359 using hydrological subbasins (0.36 %). On the other hand, the 200 m resolution grid-cells
360 configuration issues "moderate" or "high" warning level only in around 0.01 % of Catalonia.

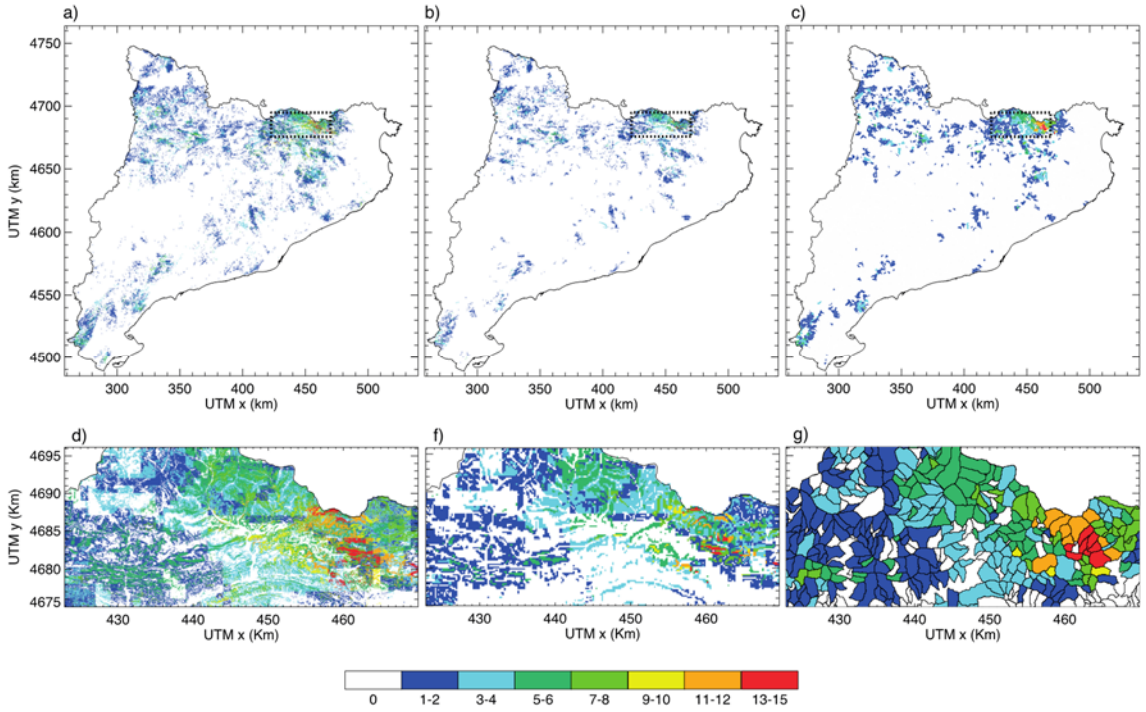


**Fig. 11.** Number of days of the period April-October 2010 during which "moderate" and "high" warning levels where issued (at least for a 30-minutes time step of the day). (a) pixels of 30 m, (b) pixels of 200 m, and (c) subbasins. A zoom into the area enclosed by the black dashed rectangle is portrayed in (d), (e) and (f) for the 30 m, 200 m and subbasins mapping units respectively.

**Table 4**. Percentage of Catalonia with 1 to 2, 3 to 5, 6 to 10 and more than 11 days with "moderate" or "high" warning level for three different mapping units.

| | Domain Area [km$^2$] | Percentage of Catalonia area with Moderate or High warning level | | | |
|---|---|---|---|---|---|
| | | 1-2 days | 3-5 days | 6-10 days | 11 days or more |
| dx = 30 m | 32030 | 7.52 | 1.59 | 0.09 | 0.01 |
| dx = 200 m | 32248 | 2.54 | 0.37 | 0.01 | 0.00 |
| Subbasins | 23048 | 13.99 | 3.12 | 0.36 | 0.01 |

The validation of the results of the LEWS in Catalonia is challenging because the areas with a large number of days with warning are mainly located in highly inaccessible mountainous regions. When an event occurs, it is hardly reported because typically no infrastructures, buildings or roads are affected, and no multi-temporal landslides inventories are available.

373 The number of days with warnings is a qualitative result that gives an idea that the number of
374 false positives is reasonable: warnings are generally located in the most susceptible areas that were
375 affected by important rainfall amounts and, are issued at most 15 days of the 214 days that comprise
376 the analyzed period. Alternatively, to evaluate the LEWS results using the different mapping units,
377 we have focused on some specific catchments where landslide reports were available during the
378 analyzed period.

379 *5.2. Validation in specific sites*

380 The performance of the LEWS with the different setups has been analyzed in two catchments
381 where debris flows have been detected during the analyzed period of 2010. These two monitored
382 catchments (Rebaixader and Erill) are both located in the NW-part of Catalonia (**Fig. 1**).

383 Although the Rebaixader catchment is relatively small (0.80 $km^2$), it is one of the most active
384 torrents in the Catalan Pyrenees and has been monitored since 2009 (Hürlimann et al. 2014). The
385 debris-flows initiation zone is located in a steep scarp in a lateral moraine. The catchment sediment
386 supply is assumed to be almost unlimited. During the analyzed period, the monitoring system
387 recorded the second largest debris flow since 2009 (on 11 July 2010, with an estimated volume of
388 12500 $m^3$) and also two debris floods that mobilized smaller volumes (on 21 July and 9 October
389 2010).

390 The Erill catchment, with a drainage area of 3.30 $km^2$, is close to the Rebaixader and the
391 outcropping material is similar. A monitoring station was installed in 2005 (Raïmat Quintana 2018)
392 and detected one debris flow during the studied period (on 22 July 2010).

393 The LEWS outputs show that the events reported during the 7-month period in the two
394 catchments mentioned above are generally associated with "moderate" or "high" warning levels
395 (the results are summarized in **Table 5Fig. 12** and **Fig. 12Table 5**).

396 In the Rebaixader catchment, the three recorded events were triggered by rather intense
397 rainfall episodes. All the LEWS configurations determine "moderate" or "high" warning levels, for

398 the 11 July 2010 debris flow and the 9 October 2010 debris flood (**Table 5** and **Fig. 12**a, and c).
399 However, the LEWS was not able to issue a warning for the 21 July 2010 rainfall event, when a
400 small debris flood was detected (**Table 5** and **Fig. 12**b), because the rainfall intensities were just
401 below the "very low"- "low" threshold.

402 Similarly, in the Erill catchment the recorded debris flow was triggered by intense rainfall. The
403 LEWS results show that both grid-cell configurations identify the event with a "high" warning level
404 and the subbasins configuration identifies it with a "moderate" warning level (**Fig. 12**d and **Table**
405 **5**).

406 **Table 5** Reported debris flows and/or debris floods at the Rebaixader and Erill catchments and maximum warning
407 level issued by the LEWS during each of the rainfall episodes.

| Subbasin | Subbasin susceptibility class | Reported events | Type of event | Maximum Warning Level | | |
|---|---|---|---|---|---|---|
| | | | | dx= 30 m | dx= 200 m | Subbasins |
| Rebaixader | High | 11 July 2010 | Debris flow | High | High | High |
| | | 21 July 2010 | Debris flood | Low | Low | Low |
| | | 09 October 2010 | Debris flood | Low | Moderate | Moderate |
| Erill | High | 22 July 2010 | Debris flow | High | High | Moderate |

408

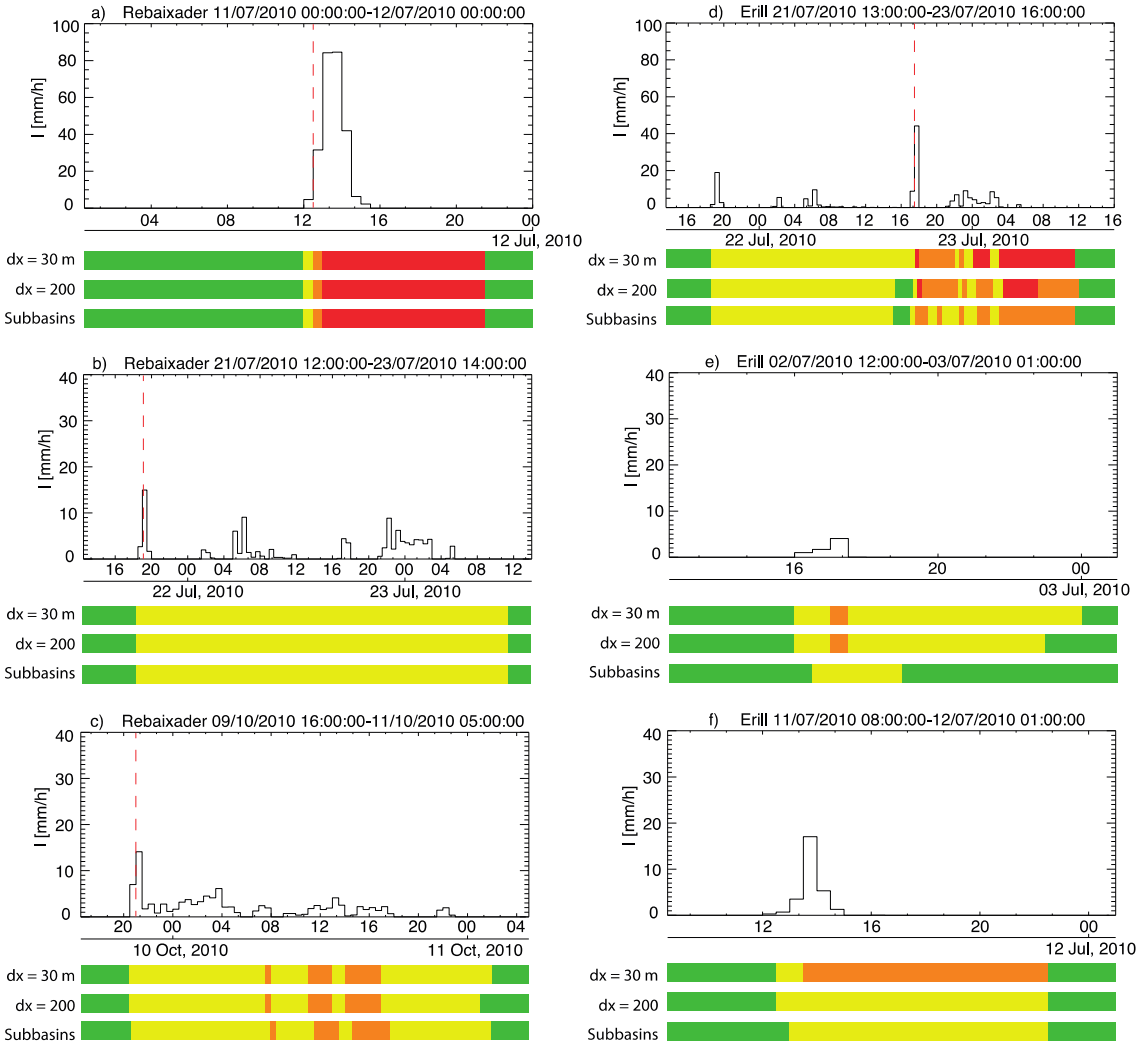


409

410 **Fig. 12.** Site-specific validation of the LEWS. At the Rebaixader monitoring site: (a) 11July 2010 debris flow, (b) 21
411 July 2010 debris flood, (c) 9 October 2010 debris flood. At Erill: (d) 22 July debris flow; and the two rainfall events
412 that did not turned on the monitoring system and (e) 2 July 2010 (f) 11 July 2010. The black line represents the 30-
413 min rainfall intensity observed by the weather radar. The horizontal color bars show the maximum warning level
414 time series observed within the catchment for the analyzed mapping units. Green, yellow, orange and red represent
415 warning levels "very low", "low", "moderate" and "high", respectively. The red dashed line indicates the time when
416 the debris flow or debris flood was detected by the monitoring station.

417 The number of recorded events at Rebaixader and Erill have been compared with the number
418 of days that achieved a maximum warning level of "moderate" or "high" classes (**Table 6**). The
419 LEWS performance at these two specific catchments has been assessed by calculating the true
420 positives, false positives, and misses, using the subbasin where the sensors where installed as the
421 mapping unit for evaluation. True positives are defined as the number of rainfall events during
422 which the monitoring systems detect a debris flow or debris flood and the LEWS issues a

423 "moderate" or "high" warning level within the catchment. False positives are rainfall events with a
424 "moderate" or "high" warning within the catchment, but during which no landslide event is
425 detected. Misses are rainfall events during which the monitoring systems record a debris flow or
426 debris flood, but the LEWS is not switching into a moderate or high warning in any mapping unit.

427 In the analyzed catchments all the tested configurations have the same number of true
428 positives and misses. However, the number of false positives seems to increase with the resolution
429 of the mapping unit, particularly in Erill (**Table 6**). The difference in the number of false positives
430 between both 30 m and 200 m grid-cell mapping units are due to the larger area classified as
431 "highly" susceptible in the 30 m grid-cell map at the the Erill catchment (**Fig. 13**a and **Fig. 13**b).

432 **Table 6** Evaluation of the performance of the LEWS for the Rebaixader and Erill monitored sites. The number of
433 recorded debris flows and debris floods can be compared with the number of days with maximum warning level
434 "moderate" or "high". True positives are rainfall events with correct warnings, false positives are rainfall events with
435 "moderate" or "high" warnings but no detected landslide, debris flow or debris flood event. Misses are rainfall events
436 with landslides, debris flows or debris floods but no "moderate" or "high" warnings.

| Monitoring site | Mapping Unit | # of days with maximum warning level | | | | #events detected | True Positives | False Positives | Misses |
|---|---|---|---|---|---|---|---|---|---|
| | | Very Low | Low | Moderate | High | | | | |
| Rebaixader | dx = 30 m | 148 | 64 | 1 | 1 | 3 | 2 | 0 | 1 |
| | dx = 200 m | 150 | 62 | 1 | 1 | | 2 | 0 | 1 |
| | Subbasins | 150 | 62 | 1 | 1 | | 2 | 0 | 1 |
| Erill | dx = 30 m | 146 | 66 | 2 | 2 | 1 | 1 | 2 | 0 |
| | dx = 200 m | 146 | 66 | 1 | 2 | | 1 | 1 | 0 |
| | Subbasins | 152 | 60 | 2 | 0 | | 1 | 0 | 0 |

437 The false positives at Erill have been further examined. Our analysis shows that the
438 significance of the false positives depends on the area (number of pixels) of the subbasin where a
439 "moderate" or "high" warning level is issued and its location. Since the monitoring station is
440 located at the catchment outlet, small landslides or debris flows happening near the headwaters and

441 traveling short distances are perhaps not detected. Therefore, false positives due to a few
442 headwaters' pixels with "moderate" or "high" warnings are not very significant. In contrast, a false
443 positive is more relevant if pixels with "moderate" or "high" warnings are located close to the
444 outlet or affect a large portion of the catchment.

445 During the analyzed period, a false positive with low significance was issued for the 11 July
446 2010 event by the 30 m grid-cell configuration at the Erill (**Fig. 12** f), when a moderate warning was
447 released. However, the moderate warning was caused by a very small area (4 % of the entire basin)
448 located in the highest part of the catchment, where the radar recorded larger amounts of rain (**Fig.**
449 **13** g). In addition, the grid-cell configurations issued another false positive that affected a portion
450 of the Erill catchment near the outlet (**Fig. 13** d and e) during the event of the 2 July 2010. However,
451 the area over which both configurations issued the warning was different. On the one hand, the
452 200 m grid-cell set-up issued "moderate" warnings over only a 1.3 % of the catchment area,
453 therefore its significance was low. On the other hand, the 30 m grid-cell set-up issued "moderate"
454 warnings over a larger area (4.8 % of the subbasin), therefore its significance was larger.

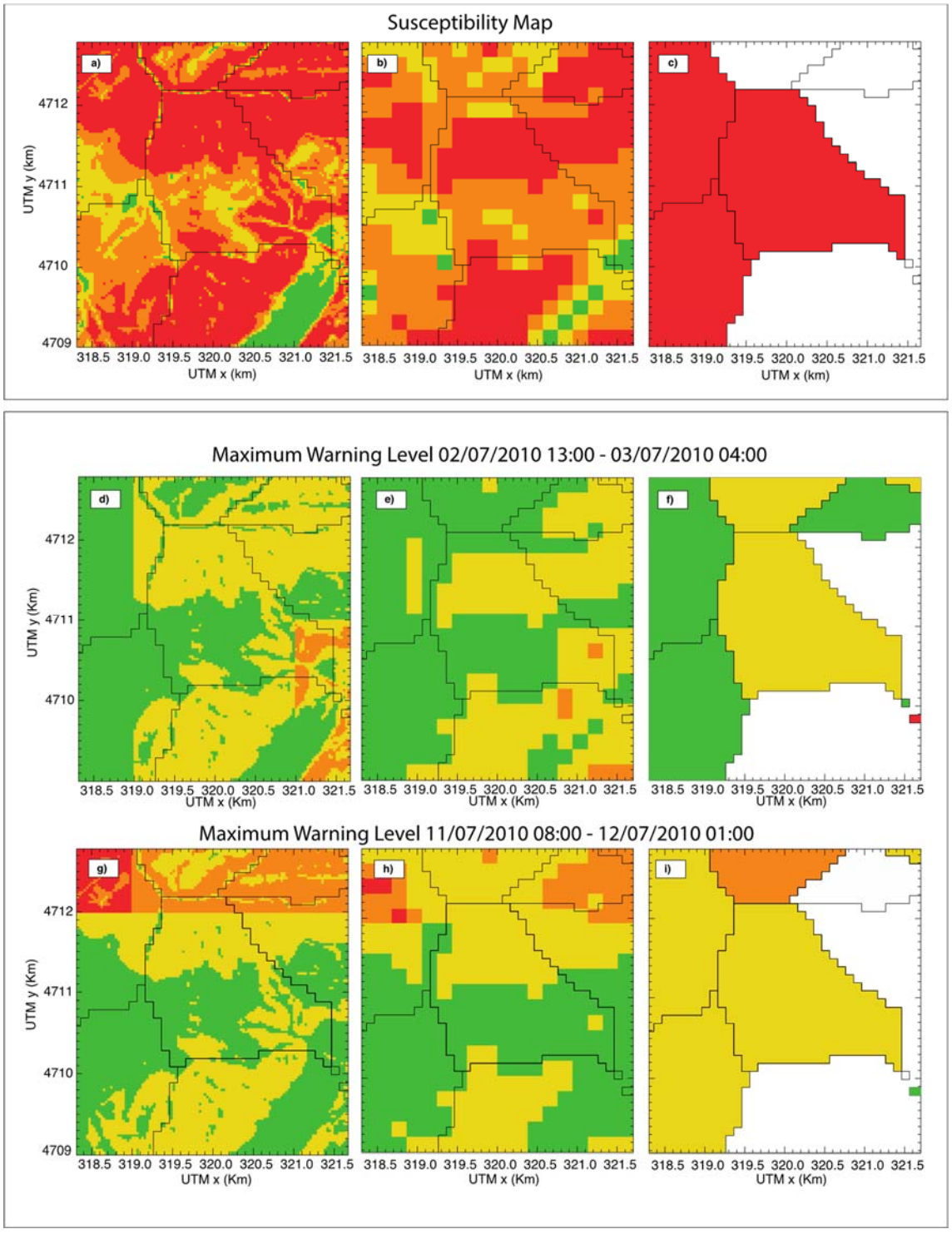


455

456 **Fig. 13.** Analysis of false positive warning issues at Erill. The top panel displays the susceptibility map based on (a)
457 30 m, (b) 200 m grid-cells, and (c) subbasin mapping units. Middle panel shows the maximum warning level for the
458 three mapping units at Erill during the 2 July 2010 rainfall event. Bottom panel presents the maximum warning level
459 for the three configurations during the July 11 July2010 rainfall. See text for detailed explanations.

460 Additionally, the outputs of the three LEWS configurations have also been checked for the
461 reported events in two supplementary unmonitored catchments, where three events were reported:

462 Portainé and Santa Maria (**Fig. 1**). The Portainé catchment has an area of 2.50 $km^2$. Two debris
463 flow events affected a secondary road and a small dam located downstream, one occurred on the
464 22 of July 2010 with a mobilized volume of 25000 $m^3$, and a smaller one on 12 August 2010 (Palau
465 et al. 2017). The Santa Maria is a 1.70 $km^2$ catchment located in the mountain of Montserrat.
466 Shallow slides and debris flows were reported there by road and railway managing authorities
467 during the night of 10 October 2010.

468 The 30 m gridded setup was able to correctly issue a "moderate" or "high" warning level
469 coinciding with the approximate time of the events in Portainé and Santa Maria (**Table 7**). On the
470 other hand, the 200 m setup failed to issue a warning for the Portainé 22 July 2010 debris flow, and
471 the subbasin setup missed both events at Portainé. The computation of the total number of true
472 positives, false positives and misses has not been possible for these two sites because only the
473 events that affected important infrastructures were reported.

474 **Table 7** Reported debris flows, debris floods and/or shallow slides at the Portainé and Santa Maria catchments and
475 maximum warning level issued by the LEWS during each of the rainfall episodes.

| Subbasin | Subbasin susceptibility class | Reported events | Type of event | Maximum Warning Level | | |
|---|---|---|---|---|---|---|
| | | | | dx= 30 m | dx= 200 m | Subbasins |
| Portainé | Moderate | 22 July 2010 | Debris flow | Moderate | Low | Low |
| | | 12 August 2010 | Debris flow | High | Moderate | Very Low |
| Santa Maria | High | 10 October 2010 | Debris flow & shallow slides | High | Moderate | Moderate |

476 In summary, the results obtained with the different configurations of the LEWS are quite similar
477 and show coherence. The main difference is the lower number of false positives obtained with the
478 subbasin setup. However, the 200 m grid-cell and the subbasin configurations also present
479 additional misses at Portainé (**Table 7**). It is worth noticing though, that one of the 30 m grid-cell

480 configuration false positives is issued over a very small area at the catchments headwaters and
481 therefore its significance is low.

482 *5.3. Computational requirements*

483 One of the criteria that strongly influences the feasibility to apply the LEWS in real time at
484 regional scale is the computational cost, which should allow us to update the warning level every
485 time new rainfall observations are available within a short time. Herein, we have analyzed the
486 computational cost to run one time step over Catalonia with the different configurations analyzed
487 in this section 5.

488 To fulfill the computations, we have used a server with two 12-cores 3.5 GHz CPUs and 48
489 GB of RAM. With the current version of the code, the time needed to fulfill one time step over
490 the entire Catalonia is around 1.5 min, 2.9 s, and 0.7 s for the case of 30 m, 200 m grid-cells and
491 subbasins respectively. The computational cost increases with the area of the domain covered by
492 rain. In either case, the three mapping units could be used to compute warnings operationally. In
493 section 4 we have decided that it is not yet feasible to run the 5 m grid over Catalonia because with
494 the current version of the codes completing the calculation of one time-step through Catalonia
495 requires around 50 min, still far from real-time requirements.

496 ## 6. Discussion and conclusions

497 This study assesses the influence of the mapping unit into the outputs of a regional scale
498 LEWS with the aim of selecting the most suitable mapping unit for a real-time LEWS for Catalonia.
499 Susceptibility maps covering Catalonia have been obtained combining the maps of slope and land
500 cover with a fuzzy logic approach. This simple methodology has been applied to obtain and
501 compare susceptibility maps based on different mapping units (pixels of several resolutions and
502 hydrological subbasins), which have been applied to run a LEWS method in the region of Catalonia
503 during seven months of 2010.

The evaluation of the susceptibility maps has been done using part of the inventory available in three subdomains in the Catalan Pyrenees and Pre-Pyrenees. The results show that for the gridded susceptibility maps, its quality decreases with resolution, whereas the one obtained on a subbasin division performs slightly better than the map based on pixels of 100 m resolution.

The analysis of the performance of the LEWS with the studied mapping units shows that landslide warnings were generally located at susceptible areas affected by large rainfall amounts. Results show that the area where the warnings were issued increases with the mapping unit resolution for the grid-cell set-ups but is higher for the subbasins configuration. Due to the lack of systematic landslide reports, the evaluation of the performance remains a challenge and has been done for specific locations with reported shallow slides and debris flow events. The subbasin setup has failed to issue a warning for three landslides that were recorded at the selected sites. The number of misses decreases with the resolution. While the 200 m grid-cell configuration misses two landslide events, the30 m grid-cell setup misses only a debris flood but has an additional false positive. However, its significance is rather low.

Regarding the computational cost, as expected, the high resolution configurations are more demanding than the coarser configurations. Regardless of that, with the exception of 5 m grid-cells, all the studied configurations could be applied in real time.

Choosing the most appropriate mapping unit for operational LEWS purposes is not trivial. It must include a compromise between performance, resolution and computational cost, whereas it must also consider the end-users' interpretability of the warnings. In this sense, at a regional scale the interpretation of the warnings is much easier for the subbasins configuration. However, grid-cell configurations have a higher resolution and display the possible landslide initiation zones with more detail.

Based on the results obtained for the analyzed period and monitored sites (a more extensive evaluation over longer periods of time and with a larger number of landslide reports would be

529 required to make the results more conclusive), the best option may be working with 30-m grid cells
530 to compute the warnings and present them in subbasins displaying the maximum warning level of
531 the enclosed pixels. This approach simplifies the assessment at regional scale without losing the
532 extra information contained in the pixel data. If a warning is issued for a given catchment, detailed
533 information on the possible landslide triggering areas can be displayed when zooming into it. Thus,
534 this solution enhances the understanding of the situation and enables to allocate the available
535 resources in the most problematic places. A similar solution has been adopted in the SIGMA model
536 (Segoni et al. 2018) where three types of mapping units are used (alert zones, municipalities and
537 100 m grid-cells).

538 One aspect that is fundamental to guarantee the performance of the LEWS is the quality of
539 the rainfall inputs. In this regard, the use of radar QPE has clear advantages (i.e. good depiction of
540 the variability of the rainfall field at high spatio-temporal resolutions), but it also needs careful
541 processing of radar observations to guarantee the quantitative value of the rainfall products (e.g.
542 Zawadzki 1984; Corral et al. 2009; Borga et al. 2014), since global or local biases of the rainfall field
543 have a direct effect on the performance of the LEWS (it may lead to false positives and misses). It
544 is also worth noting that the spatial resolution of the rainfall inputs (1 km) is much coarser than
545 that of the LEWS (which matches the resolution of the susceptibility map). This difference, which
546 can be seen in **Fig. 13**, implies that the small-scale variability of the rainfall field cannot be resolved
547 and an adds uncertainty in the performance of the LEWS.

548 A limitation of the current LEWS methodology is the lack of well-established rainfall
549 thresholds in Catalonia. Therefore, IDF-curves of a meteorological station were used to determine
550 the rainfall hazard level. However, future advances on critical rainfall conditions in Catalonia would
551 certainly improve the performance of the LEWS. An additional drawback is that the current
552 thresholds account for neither the antecedent rainfall nor soil moisture conditions. Using regional
553 rainfall thresholds for landslides, as well as including antecedent rainfall or soil moisture

554 information could help reducing the number of false positives and therefore improve the
555 performance of the LEWS (Mirus et al. 2018; Bogaard and Greco 2018).

556 Another important factor that could help improve the performance of the LEWS would be
557 the distinction between weathering limited and sediment unlimited catchments. Weathering limited
558 catchments require a certain period between debris-flow events to recharge the available sediment.
559 Currently the input susceptibility maps are static, and therefore, this condition is not considered by
560 the LEWS

561 Additionally, since most shallow slides and debris flows happen during or shortly after the
562 triggering rainfall event to issue effective early warnings the presented methodology should be
563 implemented in real-time using rainfall forecasts (Alfieri et al. 2012), for instance based on radar
564 nowcasts (e.g. Berenguer et al. 2011) or high-resolution numerical weather prediction.

565 ## Acknowledgements

566 This work has been partially funded by the EC H2020 project ANYWHERE (DRS-01-2015-
567 700099) and the Spanish project SMuCPhy (BIA 2015-67500-R). Also, the first author is supported
568 by a grant from the Secretariat of Universities and Research of the Ministry of business and
569 knowledge of the Generalitat de Catalunya. The authors acknowledge the Catalan Weather Service
570 (SMC) for providing the radar data.

571

572 **References**


573 Abancó C, Hürlimann M, Moya J, Berenguer M (2016) Critical rainfall conditions for the initiation
574 of torrential flows. Results from the Rebaixader catchment (Central Pyrenees). J Hydrol
575 541:218–229 . https://doi.org/10.1016/j.jhydrol.2016.01.019

576 Alcántara-Ayala I, Murray V, Daniels P, McBean G (2017) International Council for Science
577 (ICSU)-On the future challanges for the integration of science into international policy
578 developement for landlide disaster risk reduction. Adv Cult Living with Landslides 5:1–557 .
579 https://doi.org/10.1007/978-3-319-53483-1

580 Aleotti P (2004) A warning system for rainfall-induced shallow failures. Eng Geol 73:247–265

581 Alfieri L, Salamon P, Pappenberger F, Wetterhall F, Thielen J (2012) Operational early warning
582 systems for water-related hazards in Europe. Environ Sci Policy 21:35–49 .
583 https://doi.org/10.1016/j.envsci.2012.01.008

584 Baum RL, Godt JW (2010) Early warning of rainfall-induced shallow landslides and debris flows
585 in the USA. Landslides 7:259–272 . https://doi.org/10.1007/s10346-009-0177-0

586 Berastegui X, Casas JM, Liesa M, Losantos M, Martínez A, Muñoz JA, Roca E (2010) Històtria
587 geològica de Catalunya. Atles geològic de Catalunya 68–77

588 Berenguer M, Sempere-Torres D, Hürlimann M (2015) Debris-flow forecasting at regional scale
589 by combining susceptibility mapping and radar rainfall. Nat Hazards Earth Syst Sci 15:587–
590 602 . https://doi.org/10.5194/nhess-15-587-2015

591 Berenguer M, Sempere-Torres D, Pegram GGS (2011) SBMcast - An ensemble nowcasting
592 technique to assess the uncertainty in rainfall forecasts by Lagrangian extrapolation. J Hydrol
593 404:226–240 . https://doi.org/10.1016/j.jhydrol.2011.04.033

594 Berti M, Martina MLV, Franceschini S, Pignone S, Simoni A, Pizziolo M (2015) Implementation
595 of a probabilistic model of landslide occurrence on a civil protection alert system at regional

scale. In: Engineering Geology for Society and Territory - Volume 2: Landslide Processes. pp 659–662

Bogaard T, Greco R (2018) Invited perspectives: Hydrological perspectives on precipitation intensity-duration thresholds for landslide initiation: proposing hydro-meteorological thresholds. Nat Hazards Earth Syst Sci 18:31–39 . https://doi.org/10.5194/nhess-18-31-2018

Borga M, Stoffel M, Marchi L, Marra F, Jakob M (2014) Hydrogeomorphic response to extreme rainfall in headwater systems: Flash floods and debris flows. J Hydrol 518:194–205 . https://doi.org/10.1016/j.jhydrol.2014.05.022

Bregoli F, Medina V, Chevalier G, Hürlimann M, Bateman A (2015) Debris-flow susceptibility assessment at regional scale: Validation on an alpine environment. Landslides 12:437–454 . https://doi.org/10.1007/s10346-014-0493-x

Calvello M, Cascini L, Mastroianni S (2013) Landslide zoning over large areas from a sample inventory by means of scale-dependent terrain units. Geomorphology 182:33–48 . https://doi.org/10.1016/j.geomorph.2012.10.026

Calvello M, d'Orsi RN, Piciullo L, Paes N, Magalhaes M, Lacerda WA (2014) The Rio de Janeiro early warning system for rainfall-induced landslides: Analysis of performance for the years 2010-2013. Int J Disaster Risk Reduct 12:3–15 . https://doi.org/10.1016/j.ijdrr.2014.10.005

Carrara A, Crosta G, Frattini P (2007) Comparing models of debris-flow susceptibility in the alpine environment. Geomorphology 94:353–378 . https://doi.org/10.1016/j.geomorph.2006.10.033

Casas MC, Codina B, Redano A, Lorente J (2004) A methodology to classify extreme rainfall events in the western mediterranean area. Theor Appl Climatol 77:139–150 . https://doi.org/10.1007/s00704-003-0003-x

620 Chen C, Lin LL, Yu F, Lee C, Tseng TC, Wang AW, Kei-wai C (2007) Improving debris flow
621 monitoring in Taiwan by using high-resolution rainfall products from QPESUMS. Nat
622 Hazards 447–461 . https://doi.org/10.1007/s11069-006-9004-2

623 Chevalier G, Medina V, Hürlimann M, Bateman A (2013) Debris-flow susceptibility analysis using
624 fluvio-morphological parameters: Application to the Central-Eastern Pyrenees. Nat Hazards
625 67:213–238 . https://doi.org/DOI 10.1007/s11069-013-0568-3

626 Chevalier GG (2013) Assessing debris-flow hazard focusing on statistical morpho-fluvial
627 susceptibility models and magnitude-frequency relationships : application to the central-
628 eastern Pyrenees. TDX (Tesis Dr en Xarxa)

629 Ciurleo M, Calvello M, Cascini L (2016) Susceptibility zoning of shallow landslides in fine grained
630 soils by statistical methods. Catena 139:250–264 .
631 https://doi.org/10.1016/j.catena.2015.12.017

632 Corominas C (2000) Landslides and climate. 8th Int Symp Landslides 1–33

633 Corominas J, Moya J, Hürlimann M (2002) Landslide rainfall triggers in the Spanish Eastern
634 Pyrenees. In: 4th EGS Plinius Conference "Mediterranean Storms." Editrice, Mallorca, Spain,
635 pp 1–4

636 Corral C, Velasco D, Forcadell D, Sempere-Torres D, Velasco E (2009) Advances in radar-based
637 flood warning systems . The EHIMI system and the experience in the Besòs flash-flood pilot
638 basin. Flood Risk Manag Res Pract Ext Abstr Vol 332 Pages Full Pap CDROM 1772 Pages
639 1295–1303

640 CREAF (2009) Mapa de Cobertes del Sòl de Catalunya (MSC-4), V4 edn.

641 EEA (1990) CORINE land cover - contents. CORINE L Cover 1–163

642 Fawcett T (2006) An introduction to ROC analysis. Pattern Recognit Lett 27:861–874

643 Fell R, Corominas J, Bonnard C, Cascini L, Leroi E, Savage WZ, and on behalf of the JTC-1 Joint

644 Technical Committee on Landslides and Engineered Slopes (2008) Guidelines for landslide
645 susceptibility, hazard and risk zoning for land use planning. Eng Geol 102:85–98

646 Froude MJ, Petley DN (2018) Global fatal landslide occurrence from 2004 to 2016. Nat Hazards
647 Earth Syst Sci 18:2161–2181 . https://doi.org/10.5194/nhess-18-2161-2018

648 Gallart F, Clotet N (1988) Some aspects of the geomorphic processes triggered by an extreme
649 rainfall event: the November 1982 flood in Eastern Pyrenees. Catena Suppl 79–95

650 Gariano SL, Guzzetti F (2016) Landslides in a changing climate. Earth-Science Rev 162:227–252 .
651 https://doi.org/10.1016/j.earscirev.2016.08.011

652 Gariano SL, Petrucci O, Rianna G, Santini M, Guzzetti F (2018) Impacts of past and future land
653 changes on landslides in southern Italy. Reg Environ Chang 18:437–449 .
654 https://doi.org/10.1007/s10113-017-1210-9

655 Guzzetti F, Peruccacci S, Rossi M, Stark CP (2008) The rainfall intensity–duration control of
656 shallow landslides and debris flows: an update. Landslides 5:3–17 .
657 https://doi.org/10.1007/s10346-007-0112-1

658 Hansen MJ (1984) Strategies for classification of landslides. In: Brunsden D (ed) Slope Instability.
659 John Wiley, Chichester, pp 1–25

660 Huat LT, Ali F, Osman AR, Rahman NA (2012) Web Based Real Time Monitoring System Along
661 North-South Expressway , Malaysia. Electron J Geothechnical Eng 17:623–632

662 Hürlimann M, Abancó C, Moya J, Vilajosana I (2014) Results and experiences gathered at the
663 Rebaixader debris-flow monitoring site, Central Pyrenees, Spain. Landslides 11:939–953

664 Hürlimann M, Lantada N, Gonzalez M, Pinyol J (2016) Susceptibility assessment of rainfall-
665 triggered flows and slides in the Central-Eastern Pyrenees. In: Aversa S, Cascini L, Picarelli L,
666 Scavia C (eds) XII Int. Symposium on Landslides and Engineered Slopes. CRC Press, Naples,
667 pp 1129–1136

668 Hürlimann M, Palau RM, Berenguer M, Pinyol J (2017) Analysis of the rainfall conditions inducing
669 torrential activity in the Portainé catchment (Eastern Pyrenees, Spain). Geophys Res Abstr
670 19:12494

671 ICGC (2013) Model d'Elevacions del Terreny de Catalunya 5x5metres v1.0 (MET-5 v1.0). ICGC

672 Jakob M, Hungr O (2005) Debris flow Hazards and Related Phenomena. Springer, Berlin

673 Kirschbaum D, Stanley T (2018) Satellite-Based Assessment of Rainfall-Triggered Landslide
674 Hazard for Situational Awareness. Earth's Futur 6:505–523 .
675 https://doi.org/10.1002/2017EF000715

676 Kirschbaum D, Stanley T, Yatheendradas S (2016) Modeling landslide susceptibility over large
677 regions with fuzzy overlay. Landslides 13:485–496 . https://doi.org/10.1007/s10346-015-
678 0577-2

679 Krøgli IK, Devoli G, Colleuille H, Boje S, Sund M, Engen IK (2018) The Norwegian forecasting
680 and warning service for rainfall- and snowmelt-induced landslides. Nat Hazards Earth Syst
681 Sci 18:1427–1450 . https://doi.org/10.5194/nhess-18-1427-2018

682 Leopold P, Heiss G, Petschko H, Bell R, Glade T (2013) Susceptibility maps for landslides using
683 different modelling approaches. Landslide Sci Pract Landslide Invent Susceptibility Hazard
684 Zo 1:353–356 . https://doi.org/10.1007/978-3-642-31325-7-46

685 Liao Z, Hong Y, Wang J, Fukuoka H, Sassa K, Karnawati D, Fathani F (2010) Prototyping an
686 experimental early warning system for rainfall-induced landslides in Indonesia using satellite
687 remote sensing and geospatial datasets. Landslides 7:317–324 .
688 https://doi.org/10.1007/s10346-010-0219-7

689 Liu C, Li W, Wu H, Lu P, Sang K, Sun W, Chen W, Hong Y, Li R (2013) Susceptibility evaluation
690 and mapping of China's landslides based on multi-source data. Nat Hazards 69:1477–1495 .
691 https://doi.org/10.1007/s11069-013-0759-y

692 Lloyd DM, Wilkinson PL, A. M O, M. G. Anderson (2001) Predicting landslides: Assessment of
693 an automated rainfall based landslide warning system. In: KKS H, KS L (eds) 14th South East
694 Asia Geothecnical Conference. Balkema, Hong Kong, pp 135–139

695 Marra F, Nikolopoulos EI, Creutin JD, Borga M (2014) Radar rainfall estimation for the
696 identification of debris-flow occurrence thresholds. J Hydrol 519:1607–1619 .
697 https://doi.org/10.1016/j.jhydrol.2014.09.039

698 Mendel JM (1995) Fuzzy Logic Systems for Engineering : A tutorial. Proc IEEE 83:345–377 .
699 https://doi.org/10.1109/5.364485

700 Mirus B, Morphew M, Smith J (2018) Developing Hydro-Meteorological Thresholds for Shallow
701 Landslide Initiation and Early Warning. Water 10:1274 . https://doi.org/10.3390/w10091274

702 Nadim F, Kjekstad O, Peduzzi P, Herold C, Jaedicke C (2006) Global landslide and avalanche
703 hotspots. Landslides 3:159–173 . https://doi.org/10.1007/s10346-006-0036-1

704 NOAA-USGS Debris Flow Task Force (2005) NOAA-USGS Debris-Flow Warning System - Final
705 Report

706 Osanai N, Shimizu T, Kuramoto K, Kojima S, Noro T (2010) Japanese early-warning for debris
707 flows and slope failures using rainfall indices with Radial Basis Function Network. Landslides
708 7:325–338 . https://doi.org/10.1007/s10346-010-0229-5

709 Palau RM, Hürlimann M, Pinyol J, Moya J, Victoriano A, Génova M, Puig-Polo C (2017) Recent
710 debris flows in the Portainé catchment (Eastern Pyrenees, Spain): analysis of monitoring and
711 field data focussing on the 2015 event. Landslides 14: . https://doi.org/10.1007/s10346-017-
712 0832-9

713 Pan HL, Jiang YJ, Wang J, Ou GQ (2018) Rainfall threshold calculation for debris flow early
714 warning in areas with scarcity of data. Nat Hazards Earth Syst Sci 18:1395–1409 .
715 https://doi.org/10.5194/nhess-18-1395-2018

716 Papa MN, Medina V, Ciervo F, Bateman A (2013) Derivation of critical rainfall thresholds for
717 shallow landslides as a tool for debris flow early warning systems. Hydrol Earth Syst Sci
718 17:4095–4107 . https://doi.org/10.5194/hess-17-4095-2013

719 Persichillo MG, Bordoni M, Meisina C (2017) The role of land use changes in the distribution of
720 shallow landslides. Sci Total Environ 574:924–937 .
721 https://doi.org/10.1016/j.scitotenv.2016.09.125

722 Piciullo L, Gariano SL, Melillo M, Brunetti MT, Peruccacci S, Guzzetti F, Calvello M (2017)
723 Definition and performance of a threshold-based regional early warning model for rainfall-
724 induced landslides. Landslides 14:995–1008 . https://doi.org/10.1007/s10346-016-0750-2

725 Pisano L, Zumpano V, Malek, Rosskopf CM, Parise M (2017) Variations in the susceptibility to
726 landslides, as a consequence of land cover changes: A look to the past, and another towards
727 the future. Sci Total Environ 601–602:1147–1159 .
728 https://doi.org/10.1016/j.scitotenv.2017.05.231

729 Portilla M, Chevalier G, Hürlimann M (2010a) Description and analysis of major mass movements
730 occurred during 2008 in the Eastern Pyrenees. Nat Hazards Earth Syst Sci 10:1635–1645 .
731 https://doi.org/10.5194/nhess-10-1635-2010

732 Portilla M, Chevalier G, Hürlimann M (2010b) Description and analysis of the debris flows
733 occurred during 2008 in the Eastern Pyrenees. Nat Hazards Earth Syst Sci 10:1635–1645 .
734 https://doi.org/10.5194/nhess-10-1635-2010

735 Portilla Gamboa ME (2014) Reconstrucción y análisis de ocurrencias regionales de múltiples
736 eventos de movimientos en masa generados por lluvias históricas en los Pirineos. Tesi Dr

737 Raïmat Quintana C (2018) Dinámica y peligrosidad de las corrientes de derrubios : aplicación en el
738 barranco de Erill, Pirineo catalán. TDX (Tesis Dr en Xarxa)

739 Rossi M, Luciani S, Valigi D, Kirschbaum D, Brunetti MT, Peruccacci S, Guzzetti F (2017)

740 Statistical approaches for the definition of landslide rainfall thresholds and their uncertainty
741 using rain gauge and satellite data. Geomorphology 285:16–27 .
742 https://doi.org/10.1016/j.geomorph.2017.02.001

743 Schmidt KM, Roering JJ, Stock JD, Dietrich WE, Montgomery DR, Schaub T (2002) The
744 variability of root cohesion as an influence on shallow landslide susceptibility in the Oregon
745 Coast Range. Can Geotech J 38:995–1024 . https://doi.org/10.1139/cgj-38-5-995

746 Schwarz M, Preti F, Giadrossich F, Lehmann P, Or D (2010) Quantifying the role of vegetation in
747 slope stability: a case study in Tuscany (Italy). Ecol Eng 36:285–291 .
748 https://doi.org/10.1016/j.ecoleng.2009.06.014

749 Segoni S, Rosi A, Fanti R, Gallucci A, Monni A, Casagli N (2018) A Regional-Scale Landslide
750 Warning System Based on 20 Years of Operational Experience. 1–17 .
751 https://doi.org/10.3390/w10101297

752 Shu H, Hürlimann M, Molowny-Horas R, González M, Pinyol J, Ma J (2019) Relation between
753 land cover and landslide susceptibility in Val d'Aran, Pyrenees (Spain): historical aspects,
754 present situation and forward prediction. Sci Total Environ 133557

755 Strahler AN (1957) Quantitative Analysis of Watershed Geomorphology. EOS, Trans - Am
756 Geophys Union 38:913–920 . https://doi.org/10.1029/tr038i006p00913

757 UNISDR (2015) Sendai Framework for Disaster Risk Reduction. In: Third United Nations World
758 Conference on Disaster Risk Reduction. pp 1–25

759 Wilde M, Günther A, Reichenbach P, Malet J-P, Hervás J (2018) Pan-European landslide
760 susceptibility mapping: ELSUS Version 2. J Maps 14:97–104 .
761 https://doi.org/10.1080/17445647.2018.1432511

762 Yin K, Chen L, Zhang G (2008) Regional Landslide Hazard Warning and Risk Assessment. Earth
763 Sci Front 14:85–93 . https://doi.org/10.1016/s1872-5791(08)60005-6

764 Zawadzki I (1984) Factors Affecting the Precision of Radar Measurements of Rain. In: 22nd
765 Conference on Radar Meteorology. American Meteorological Society, Zurich (Switzerland),
766 pp 251–256

767